Dalton Transactions

Accepted Manuscript

ROYAL SOCIETY OF CHEMISTRY

www.rsc.org/dalton

Nuclease activity and interaction studies of unsymmetrical binuclear Ni(II) complexes with CT-DNA and BSA

S. Poornima[a], K. Gunasekaran[b] and M. Kandaswamy[a*]

Abstract

New unsymmetrical binuclear Nickel(II) complexes $[Ni_2L^{1-5}](ClO_4)_2$ (**1 - 5**) were synthesized by using [NiL] [(3-((9E)-(2-((E)-(3-formyl-2-olato-5-methylbenzylideneamino)methyl) phenylimino)methyl)-3-formyl-5-methyl-2-olato)nickel(II)] with various diamines like 1,2-diamino ethane (L^1), 1,3-diamino propane (L^2), 1,4-diamino butane (L^3), 1,2-diamino benzene (L^4) and 1,8-diamino naphthalene (L^5) and characterized by elemental analysis and spectroscopic methods. The molecular structure of binuclear nickel(II) complex **1** are determined by single crystal X–ray diffraction method. Cyclic voltammogram of binuclear Ni(II) complexes exhibit two quasi-reversible reduction waves in the cathodic region and two oxidation waves in the anodic region. DNA binding, protein binding and DNA cleavage studies were investigated. The interactions of the complexes (**1 – 5)** with calf thymus DNA were studied by spectroscopic techniques, including absorption and fluorescence methods. The binding affinities of the complexes (**1 – 5)** with CT-DNA and nuclease activities are in the following order: **5** > **4** > **3** > **2** > **1**. Binuclear Ni(II) complex **1** cleaved the plasmid DNA by hydrolytic path way. The hydrolytic cleavage of DNA by the complexes is supported by the evidence from free radical quenching and T4 ligase ligation. Binuclear Ni(II) complexes (**1-5)** displayed significant protein (Bovine Serum Albumin) interaction. Experimental results showed that the interaction between binuclear Ni(II) complexes and BSA was mainly a static quenching process.

Key words: macrocyclic binuclear Ni(II) complexes, DNA binding studies, BSA binding studies, DNA cleavage studies.

1. Introduction

Cisplatin is a widely used anticancer drug that is highly effective against testicular and ovarian cancers but has a number of side effects such as nephrotoxicity, ototoxicity, and allergy and a limited spectrum of activity due to inherent and/or acquired resistance.[1] This is an impetus to inorganic chemists to develop innovative strategies for the preparation of more effective, less toxic, target specific, and preferably noncovalently bound anticancer drugs. Many studies suggest that DNA is the primary intracellular target of antitumor drugs, because the interaction between small molecules and DNA can cause DNA damage in cancer cells.[2-4] The metallo-intercalators tend to be strongly mutagenic, and some have shown promising chemotherapeutic activity, which correlates well with DNA-binding affinity.[5-8] The search for low molecular weight molecules able to catalytically cleave DNA has attracted much interest among scientists, although a great number of nucleases are well-known. This interest embraces the elucidation of the cleavage mechanism, the role of metals in biological systems, and the design of more effective synthetic hydrolases, as well as the use of these new compounds as catalysts, conformational probes, and synthetic restriction enzymes.[9] In particular, certain Ni(II) complexes, which strongly bind and cleave DNA, exhibited prominent anticancer activities and regulate apoptosis.[10] However, these studies, are mainly limited to mononuclear complexes and very few studies on dinuclear Ni(II) complexes have been reported so far.[11] In our previous reports, we have demonstrated that some of the binuclear Ni(II), VO(II), Cu(II) and Zn(II) complexes displayed better DNA hydrolysis than their mononuclear analogs.[12,13] On the other hand, serum albumins, as the most abundant proteins in the circulatory system, act as transporter and disposer of many endogenous and exogenous compounds.[14] Bovine serum albumin (BSA) is structurally homologous to human serum albumin (HSA).[15] The affinities of drugs to protein would directly influence the concentration of drugs in the blood and in the binding sites and the duration of the effectual drugs and consequently contribute to their magnitude of biological actions in vivo. The binding of drugs to serum albumin in vitro, considered as a model in protein chemistry to study the binding behavior of proteins, has been an interesting research field in chemistry, life sciences, and clinical medicine.[16] This led to search for other modalities that interacting BSA is essential. Keeping these things in mind, we have synthesized a series of targeting new macrocyclic binuclear nickel(II) complexes (**Scheme 1**) and investigated their electrochemical, DNA and BSA interaction properties.

2. Results and discussion

2.1 Structural analysis of Ni(II) complexes

IR spectra of mononuclear complex [NiL] exhibited a peak at 1619 cm^{-1} is due to the azomethine group (C=N) present in the complex. The band observed at 1668 cm^{-1} is due to the aldehyde group (C=O). The O-H stretching frequency was not observed around 3350 cm^{-1} which indicates that phenolic O-H is deprotonated may be due to complex formation. The carbonyl stretching frequency ν(C=O) was not observed in the binuclear complex which indicates that Schiff base condensation and showed a peak around 1620 to 1640 cm^{-1} is due to the stretching frequency of azomethine group ν(C=N). The IR spectra of the binuclear complexes showed a strong band in the region around 1070–1110 cm^{-1} and a sharp peak in the region around 626 cm^{-1}, which could be due to the antisymmetric stretch and antisymmetric bending vibration of perchlorate ions, respectively. The broad band observed around 3340 cm^{-1} due to coordinated or lattice water in the binuclear complexes. The absorption spectra

[a]*Department of Inorganic chemistry,University of Madras, Maraimalai Campus, Guindy, Chennai-600025, India. E–mail: mkands@yahoo.com; Fax: +91–44–22300488.*

[b]*Centre of Advanced Study in Crystallography and Biophysics, University of Madras, Maraimalai Campus, Guindy, Chennai-600025, India. E–mail: mkands@yahoo.com; Fax: +91–44–22300488.*

of all the complexes in CH_3CN, displayed three bands over the range 500-900 nm. These are the characteristic of Ni^{2+} in the six coordination environment.[17] These are assigned to the $3A_{2g} \rightarrow 3T_{1g}$ (P), $3T_{1g}$ (F) and $3T_{2g}$ (F) transitions, respectively.[18] ESI-MS spectrum of unsymmetrical binuclear complexes showed a peak at m/z 653, 667, 681, 701 and 751 have been assigned to the $[L^{1-5}+2Ni+ClO_4]^+$ ion, respectively.

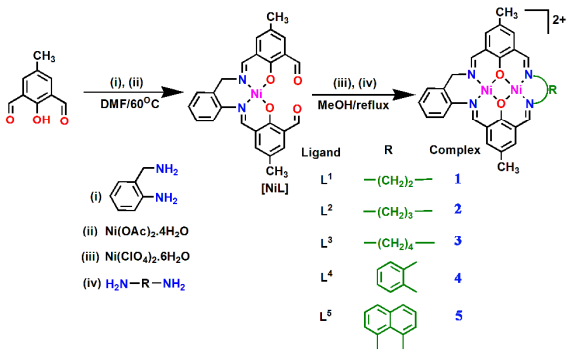

Scheme 1. Synthesis of binuclear Ni(II) complexes

2.2. Description of crystal structure of complex 1

Complex 1 crystallizes in triclinic space group P-1. The structure was refined to a final R factor of 4.57%. In the complex, one Ni ion seems to have octahedral coordination whereas the other Ni is found to be with square planar arrangement. The selected bond length and angles are given in table (Table. 1). Both the Ni ions are bridged by two phenol oxygen atoms (O1 and O2). Both the Ni ions and their ligating atoms from the macro cyclic ligand lie in a plane. In addition to this, one water molecule and aceto-nitrile occupy the fifth and sixth coordination sites around Ni2 ion. The coordination sphere around both the Ni1 and Ni2 ions lay within the allowed geometrical values except N1-Ni2-N2. The N1-Ni2-N2 angle is around 100 degrees which is a slight deviation from regular octahedral geometry and that can be justified by the bulky substitution by which N1 and N2 are connected. In the crystal structure, one asymmetric unit seems to possess an additional aceto-nitrile molecule and a water molecule along with two per chlorate ions.
The Ni1 coordination is slightly stronger than the Ni2 which can be evident by the Ni-ligand distances (Table.1(a)). The higher thermal parameter of O1W and the disordered coordinated aceto-nitrile C1' explain their free vibrations around their mean positions. The thermal parameters of O3, O5 and O6 explain a high degree of free rotation of the Cl1-O4 bond. In the other per chlorate ion, all the oxygen atoms found to be disordered.

The ligated water molecules form a strong O-H…O hydrogen bond with isolated water molecule (O1W) and Nitrogen atom of isolated aceto-nitrile (N6) in the lattice.

O1L-H2L … O1W 2.645(6) A with D-H…A angle of 173(4)
O1L-H1L … N6 (1-x, 1-y, 1-z) 2.857 A with D-H…A angle of 156(2)

As difference Fourier map did not yield clear electron density, hydrogen atoms for isolated water molecule could not be located.

Fig. 1. Thermal ellipsoid plot of complex **1** with 50% probability level. The isolated water molecule, perchlorate ions, acetonitrile and hydrogen atoms were omitted for clarity.

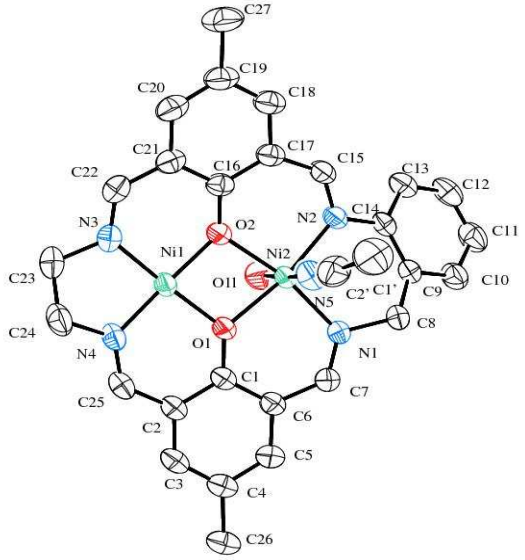

Table 1: (a) Selected geometries around Ni(II) ions in complex 1; (b) Hydrogen bonding details

a) Selected geometries around the metal ions

Atoms	distance (A)	Atoms	distance (A)
Ni1—Ni2	2.9552 (5)		
Ni1—N3	1.827 (2)	Ni2—N1	1.959 (2)
Ni1—N4	1.828 (2)	Ni2—N2	1.997 (2)
Ni1—O1	1.845(2)	Ni2—O1L	2.091 (3)
Ni1—O2	1.856 (2)	Ni2—N5	2.187 (3)

Atoms	angle ()	Atoms	angle ()
O1—Ni1—O2	83.4(1)	O2—Ni2—O1	76.0(1)
N3- Ni1- N4	87.8(1)	O1L- Ni2 - N5	177.3(1)

b) Hydrogen bonding

O1L-H1L…O1W	O1L…O1W= 2.645(6)	D-H…A =173(4)	Intra molecular
O1L-H2L … N6	O1L…N6= 2.857(6)	D-H…A =156(2)	Inter (1-x,1-y,1-z)

2.3 Electrochemical studies

Electrochemical properties of mononuclear Ni(II) and binuclear Ni(II) complexes were studied by cyclic voltammetry in the potential range 1.6 to -1.6 V in DMF containing 0.1M TBAP and the data summarized in Table II. The cyclic voltammetric response of both oxidative and reductive waves of mononuclear Ni(II) complex was examined in a scan rate range from 25 to 100 mV s^{-1} [Fig. 2]. Fig. 2a shows reduction of Ni(II) complex with an E_{pc} = -1.18 V and Epa = -1.07 V in the cathodic region

corresponding to $Ni^{II}Ni^{I}$ redox couple. Fig. 2b shows oxidation of Ni(II) complex with an anodic peak potential E_{pa} = 0.46 V and E_{pc} = 0.37 V in the anodic region corresponds to $Ni^{II}Ni^{III}$ redox couple. ΔE values are greater than 59/n mV and increases with scan rate. The cathodic and anodic peak current ratio is greater than unity. The nature of the wave shape broadens as this scan rate increases. This indicates that the cyclic voltammetric response of both oxidative and reductive waves of Ni(II) complex are quasi-reversible in nature.

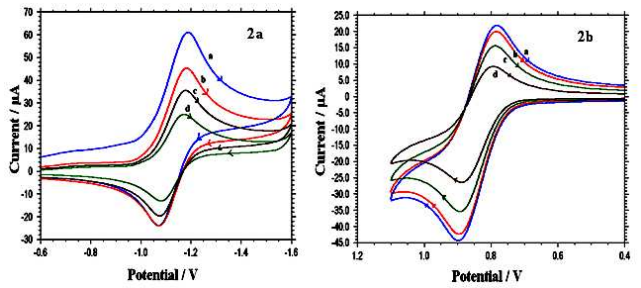

Fig. 2a Cyclic voltammogram of [NiL] complex in the cathodic region with various scan rate (a) 100 mV, (b) 75 mV, (c) 50 mV, (d) 25 mV.[NiL] = 1 x 10^{-3} M, [TBAP] = 1 x 10^{-1} M, Fig. 2b Cyclic voltammogram of [NiL] complex in the anodic region with various scan rate (a) 100 mV, (b) 75 mV, (c) 50 mV, (d) 25 mV. [NiL] = 1 x 10^{-3} M, [TBAP] = 1 x 10^{-1} M.

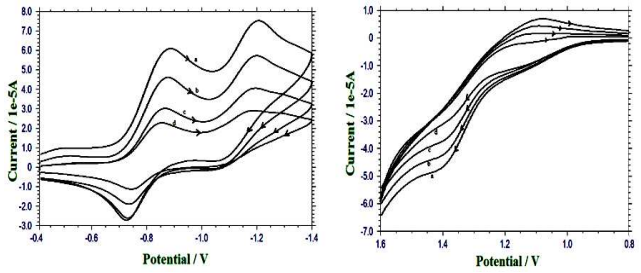

Fig. 3. (left)Cyclic voltammogram of complex **1** in the cathodic region with various scan rate (a) 100 mV, (b) 75 mV, (c) 50 mV, (d) 25 mV. [Complex **1**] = 1 x 10^{-3} M, [TBAP] = 1 × 10^{-1} M, (right) Cyclic voltammogram of complex **1** in the anodic region with various scan rate (a) 100 mV, (b) 75 mV, (c) 50 mV, (d) 25 mV. [Complex **1**] = 1 × 10^{-3} M, [TBAP] = 1 × 10^{-1} M.

The complexes **1** to **5** show two quasi-reversible reduction waves in the potential ranges E^{1}_{pc}= -0.67 to -1.31 V and E^{2}_{pc} = -0.95 to -1.55 V. The first quasi reversible signal attributed to the $Ni^{II}Ni^{II}$/ $Ni^{I}Ni^{II}$ redox couple. The second quasi-reversible wave can be attributed to the formation of the $Ni^{I}Ni^{I}$ species from the reduction of $Ni^{I}Ni^{II}$. The complex **1** showed two quasi-reversible reduction waves ($E^{1}_{1/2}$ = -0.80 V and $E^{2}_{1/2}$ = -1.15 V vs Ag/AgCl) in the cathodic region (Fig. 3). The effect of scan rate (v) on the cyclic voltammetric response, ΔE values, the cathodic and anodic peak current ratio indicates that the redox processes are quasi-reversible in nature. The two reduction peaks are associated with stepwise reducion process at metal center.

$$Ni^{II}Ni^{II} \leftrightarrow Ni^{II}Ni^{I} \leftrightarrow Ni^{I}Ni^{I}$$

Complexes **1** to **5** showed an irreversible (E^{1}_{pa}= + 0.96 V to + 1.12 V) followed by a quasi-reversible ($E^{2}_{1/2}$ = + 1.17 V to + 1.39 V vs Ag/AgCl) oxidation waves in the anodic region. In the positive potential region complex **1** showed irreversible followed by quasi-reversible oxidation waves (E^{1}_{pa} = + 1.10 V and E^{2}_{pa}= +1.37 V) in a scan rate range from 25 to 100 mV s^{-1} is shown in Fig. 3. The two oxidation peaks are associated with stepwise oxidation process at metal center.

$$Ni^{II}Ni^{II} \rightarrow Ni^{II}Ni^{III} \leftrightarrow Ni^{III}Ni^{III}$$

Two different reduction and oxidation waves of all the Ni(II) complexes may be due to Ni(II) ions present in two different compartments as well as electrostatic effects arises during redox processes. When the first Ni(II) ion is getting reduced then the charge of the complex decreases from +2 to +1. Therefore, the second Ni(II) ion reduced at higher negative potentials.[19] As the chain length of the alkylimine compartment increases, the entire macrocyclic ring becomes more flexible. The distortion around the geometry also increases. It has been suggested[20] that reduction of electron density on the metal ions and distortion in geometry favors the reduction process $Ni^{II}Ni^{I}$ at less negative potentials, as observed in the complex **1** to **3**. As the size of the macrocycle is increased, shifting of both first and second reduction potentials towards anodic is observed for the binuclear nickel(II) complexes.

Table II. The electrochemical data of the Ni(II) complexes **1-5**

	Reduction process								Oxidation process				
Complex	E_{pc}^{1} (V)	E_{pa}^{1} (V)	$E_{1/2}^{1}$ (V)	ΔE^{1} (mV)	E_{pc}^{2} (V)	E_{pa}^{2} (V)	$E_{1/2}^{2}$ (V)	ΔE^{2} (mV)	E_{pa}^{1} (V)	E_{pa}^{2} (V)	E_{pc}^{2} (V)	$E_{1/2}^{2}$ (V)	ΔE^{2} (mV)
1	-0.88	-0.73	-0.80	150	-1.20	-1.10	-1.15	100	+1.10	+1.37	+1.20	+1.29	170
2	-0.72	-0.63	-0.67	90	-0.98	-0.83	-0.90	150	+1.10	+1.38	+1.20	+1.29	180
3	-0.67	-0.47	-0.57	200	-0.95	-0.80	-0.87	150	+0.96	+1.17	+0.98	+1.06	190
4	-0.91	-0.75	-0.83	160	-1.26	-1.15	-1.20	110	+1.16	+1.36	+1.20	+1.28	160
5	-0.84	-0.66	-0.75	180	-1.15	-1.01	-1.07	150	+1.12	+1.39	+1.22	+1.31	170

Measured by Cyclic Voltammograms at 100 mV/s, E Vs Ag/AgCl. Conditions: GC working and Ag/AgCl reference electrodes; supporting electrolyte, 0.1 M, TBAP; [complex] = 1 × 10^{-3} M.

Complexes containing aromatic diimines (**4** and **5**) get reduced at higher negative potential than that of the complexes containing aliphatic diimine, the higher reduction potential can be attributed due to the greater planarity and electronic properties those are associated with aromatic rings.[21]

2.4 DNA binding studies

2.4.1 Absorption spectral studies

The interaction of Ni(II) complexes **1-5** to CT-DNA was monitored by absorption spectral titrations. Complexes **1-5** exhibited intense absorption bands around 260 nm which are assigned to л – л* transition of aromatic chromophore and at 390 nm which are attributed to metal to ligand charge transfer bands. The absorption spectra of complex **1** and **5** in the absence and

presence of CT-DNA are shown in Fig. 4. Addition of increasing amounts of CT-DNA results in an appreciable decrease in absorption intensity of complexes and in significant shift in wavelength. The absorption peaks at 251 nm for **1** and 300 nm for **5** are attributed to an intraligand л-л* transition. Upon increasing the CT-DNA concentration, hypochromism and red-shifts of 35 %, 3 nm (for **1**) and 65 %, 10 nm (for **5**) are observed for the maximal peaks. The absorption peaks at 390 nm for **1** and 455 nm for **5** which are attributed to metal to ligand charge transfer transition. Upon increasing the CT-DNA concentration, 50 % and 60 % of hypochromism, 2 nm and 6 nm of red shifts for complex **1** and **5** respectively was obtained. The binding constant K_b of Ni (II) complexes **1**-**5** can be calculated as 1.17×10^4, 2×10^4, 2×10^4, 5×10^4 and 1.16×10^5, respectively. These values suggest that the complex **5** has stronger binding affinity than the other complexes may be due to the co-planarity of the naphthalene ring system in the macrocyclic ring.

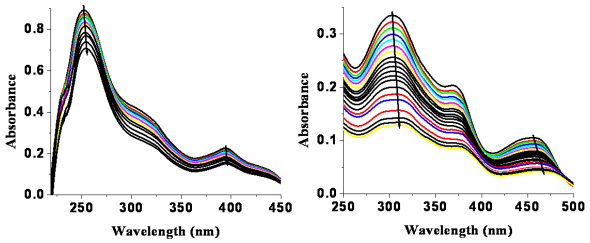

Fig. 4. Absorption spectra of the complex **1** (left) and complex **5** (right) in the absence and presence of increasing amounts of CT-DNA (0-250 μM) in Tris-HCl buffer. The arrow shows the changes on absorbance of complex upon increasing the CT-DNA concentration.

2.4.2 Fluorescence spectral studies

The fluorescence spectral method is used to study the relative binding of these complexes to CT-DNA. Ethidiumbromide emits intense fluorescence at about 600 nm in the presence of DNA because of its strong interaction between the adjacent DNA base pairs.[22]

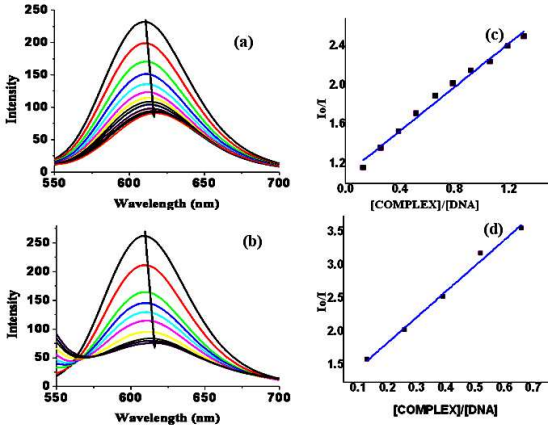

Fig. 5. Emission spectra of EB bound to DNA in Tris-HCl buffer (pH 7.2) in the absence and presence of the complex **1** (a) and **5** (b). [EB] = 4 μM, [DNA] = 40 μM, [complex **1** and **5**] = 0 to 160 μM. (λ_{ex} = 520 nm). Plot of I_0/I vs [complex]/[DNA] for fluorescence quenching curves of EB-DNA by complex **1** (c) and **5** (d).

Addition of second molecule, which binds to DNA more strongly than EB, would quench the EB-DNA by either replacing the EB or by accepting the excited-state electron of the EB through a photoelectron transfer mechanism.[23] The fluorescence quenching of EB bound to CT-DNA by complex 1 and 5 is shown in Fig. 5. The addition of complex to EB bound CT-DNA solution caused obvious reduction in emission intensities, indicating that complex competitively bound to CT-DNA with EB. It may be due to the complex interacting with DNA through intercalation binding, so releasing some free EB from the EB-DNA complex. The Stern-Volmer quenching constant K value of the complexes 1 to 5 were calculated as 1.02 (R = 0.988), 1.11(R = 0.998), 1.06 (R = 0.988), 2.92 (R = 0.984) and 3.6 (R = 0.990), respectively. The Kapp values of the complexes **1** to **5** were calculated as 4.3×10^5, 5.3×10^5, 5.8×10^5, 2.6×10^6 and 3.3×10^6 respectively. From this spectral data, complex **5** binds well through intercalative than the other complexes due to presence of aromatic naphthalene ring.

2.4.3 Viscosity measurements

Viscosity measurements were carried out to further clarify the mode of interaction of metal complexes to DNA. A classical intercalative mode causes a significant increase in viscosity of DNA solution due to increase in separation of base pairs at intercalation sites and hence an increase in overall DNA length.

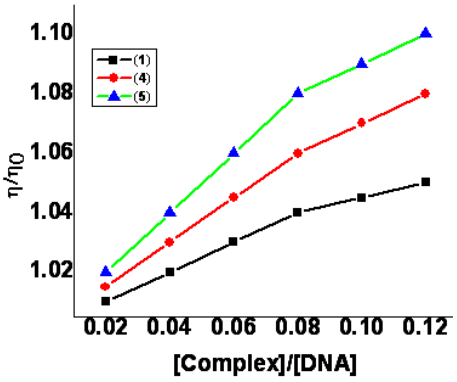

Fig. 6. Relative viscosity increments of DNA solution and complexes **1**, **4**, **5** with increasing [complex]/[DNA] ratios of 0.02 to 0.12 respectively.

As shown in Fig. 6, with increasing [complex]/[DNA] ratios from 0.02 to 0.12, the complexes **1**, **4**, **5** exhibit a tendency of increasing relative viscosity, which strongly suggests intercalation as the main binding mode of these complexes when interacted with CT-DNA. The increase in relative viscosity, expected to correlate with complex-DNA intercalating potential, followed the order **5** › **4** › **1**. This results suggest that complex **5** can binds strongly to DNA through intercalation than the other complexes, due to the presence of naphthalene ring system.

2.4 Protein binding studies

2.4.1 Fluorescence quenching of BSA by Ni(II) complexes

Fluorescence quenching refers to any process that decreases the fluorescence intensity of a fluorophore due to a variety of molecular interactions including excited-state reactions, molecular rearrangements, energy transfer, ground-state complex formation and collision quenching. Addition of the nickel (II) complexes **1-5** to BSA resulted in the quenching of fluorescence emission intensity.

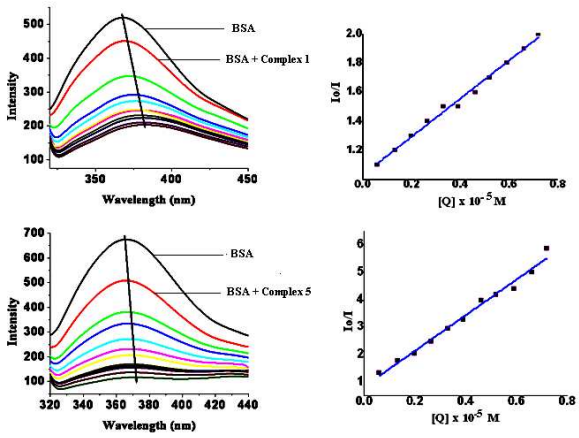

Fig. 7. Changes in the fluorescence spectra of BSA upon increasing complex (**1** and **5)** concentration at 300 K. The concentration of protein is 1.0×10^{-6} M^{-1}, and complex concentration was varied from 0.0 to 10.0×10^{-6} M^{-1}, pH = 7.5 and λ_{ex} = 280 nm. Left: Plot of I_0/I Vs [Q].

Table III. BSA binding parameters of Ni(II) complexes **1-5**

Complex	10^5K_{SV} (M^{-1})	$10^{13}K_q$[a] ($M^{-1}s^{-1}$)	10^6K_b [n][b] (M^{-1})
1	1.2×10^5	1.2×10^{13}	1.40×10^5 [0.90]
2	1.7×10^5	1.7×10^{13}	1.30×10^6[1.10]
3	2.0×10^5	2.0×10^{13}	2.00×10^5[0.96]
4	3.5×10^5	3.5×10^{13}	1.17×10^7 [1.30]
5	6.5×10^5	6.5×10^{13}	1.12×10^6 [1.00]

[a]Binding K_b (M^{-1}) and quenching K_q constants ($M^{-1}s^{-1}$) were determined by fluorescence spectral titration and [b][n] is the number of the binding sites per BSA.

The values of K_{sv} and K_q obtained for the binding of BSA to the binuclear nickel (II) complexes is given in Table III. The value of k_q, which are 1000-fold higher than the optical collision constants, 2.0×10^{10} $molL^{-1}s^{-1}$.[24] These results indicate that the specific interaction between binuclear Ni(II) complexes and protein and the probable quenching mechanism was not initiated by dynamic quenching but by a static one. The values of K indicate that there is strong binding force between the binuclear Ni(II) complexes and BSA. The values of n are approximately equal to 1, indicating that there is one class of binding site to complex in BSA.

2.4.2. Absorption spectral changes of BSA by Ni(II) complexes

A static process for the observed quenching can also be supported by the UV-vis spectra of the fluorophore. For a dynamic quenching mechanism, the absorption spectra of the fluorescent substance is not changed, and only the excited state fluorescence molecule is influenced by quenchers, while, for static quenching, a new compound is formed between the ground state of the fluorescent substance and quencher and, therefore, the absorption spectra of fluorescence substance would be considerably influenced.[25] Fig. 8 shows the UV absorption of the proteins in the presence and absence of the binuclear Ni(II) complexes. As can be seen from Fig. 8, BSA proteins possess two absorption peaks at around 220 and 280 nm. The absorbance of BSA is decreased and red shift also observed upon addition of complexes. These results show that the interaction between binuclear Ni(II) complexes and BSA was mainly a static quenching process.

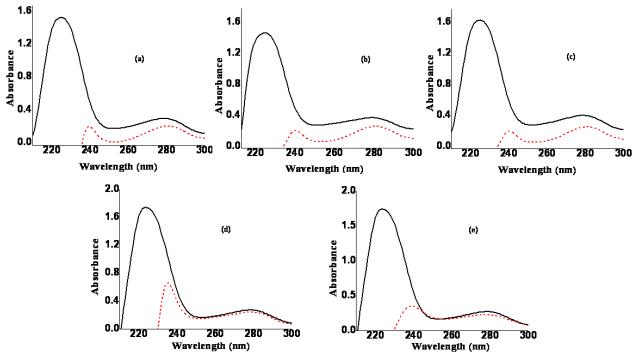

Fig. 8. UV- vis absorption spectra of BSA in the absence and presence of complex (a) **1**, (b) **2**, (c) **3**, (d) **4** and (e) **5**. Solid line: the absorption spectrum of [BSA]. Dashed line: the absorption spectrum of proteins in the presence of complexes at the same concentration, [BSA] = [complex **1-5**] = 10×10^{-6} M^{-1}.

2.5 DNA cleavage studies

The chemical nuclease activity of the complexes **1-5** has been studied using supercoiled pBR32 DNA in a medium of 50 mM Tris-HCl buffer (pH = 7.2) in the absence of external agents under physiological conditions. The results of the gel electrophoresis separations of plasmid pBR322 DNA by the complexes **1-5** are depicted in the Fig. 9. All the five complexes showed DNA cleavage activity and the aromatic diamine condensed macrocyclic Ni(II) complexes showed higher DNA cleavage activity than the aliphatic diamine condensed macrocyclic Ni(II) complexes. The structure of the ligand plays an important role in the cleavage.[26]

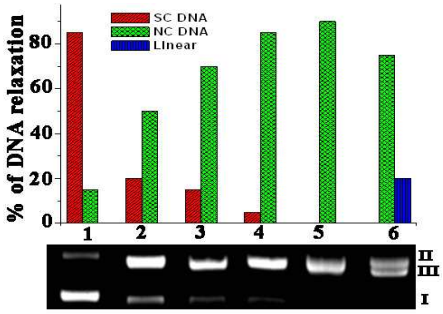

Fig. 9. Cleavage of SC pBR322 DNA by binuclear Ni(II) complexes **1** – **5** (75 μM) in Tris–HCl buffer (pH = 7.2) at 37ºC for 3 h. Lane 1, DNA control, Lane 2, DNA + Complex **1**, Lane 3, DNA + complex **2**, Lane 4, DNA + complex **3**, Lane 5, DNA + Complex **4**, Lane 6, DNA + Complex **5.**

Nickel complexes can cleave DNA through both hydrolytic and oxidative processes. For the oxidative process, the complexes have been shown to react with molecular oxygen or hydrogen peroxide to produce a variety of active oxidative intermediates (reactive oxygen species). In order to obtain information about the active oxygen species which was responsible for the DNA damage, we investigated the DNA cleavage in the presence of hydroxyl radical scavengers (DMSO, KI), singlet oxygen quenchers (L-histidine, NaN_3), superoxide scavenger (superoxide dismutase enzyme SOD) and chelating agent (EDTA) under our experimental conditions. From Fig. 10, we can see that no inhibitions are observed for the complex in the presence of DMSO (lane 3), KI (lane 4), NaN_3 (lane 6), L-histidine (lane 7) and SOD (lane 8), the results rule out the possibility of DNA cleavage by hydroxyl radical, singlet oxygen and superoxide anion. The EDTA (Lane 5), a chelating agent that strongly bind to Ni(II) forming a stable complex, can efficiently inhibit DNA cleavage, indicating Ni(II) complexes play the key role in the cleavage. In order to further clarify if the O_2 in air has effect on the DNA cleavage, it is necessary to perform the cleavage experiment under anaerobic condition, as shown in Fig. 11 (lane 2), the results showed that the complex could cleave pBR322 plasmid DNA efficiently under anaerobic condition.

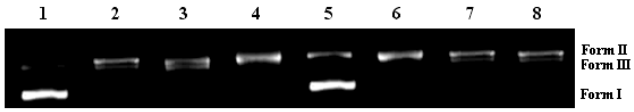

Fig. **10**. Agarose gel showing cleavage of pBR 322 DNA incubated with complex **1** (100 μM) in Tris – HCl / NaCl buffer (pH = 7.2) at 37ºC for 3 h. Lane 1, DNA control, Lane 2, DNA + Complex **1** (100 μM), Lane 3, DNA + Complex **1** (100 μM) + DMSO (2 μl), Lane 4, DNA + Complex **1** (100 μM) + KI (5 mM), Lane 5, DNA + Complex **1** (100 μM) + EDTA (5mM), Lane 6, DNA + Complex **1** (100 μM) + L-Histidine (5mM), Lane 7, DNA + Complex **1** (100 μM) + NaN_3 (5 mM), Lane 8, DNA + Complex **1** (100 μM) + SOD (4 units).

To ascertain the hydrolytic nature of the cleavage reaction, the NC and linear form obtained from the cleavage of SC DNA by complex **1 (**100 μM) was reacted with T4 ligase enzyme and we have observed complete conversion of the NC DNA and linear to its original SC form (Fig. 10).[27] The results presented here reveal that complex **1** act as a synthetic nuclease, breaks the plasmid DNA in the presence and absence of oxygen, probably through a hydrolytic mechanism.

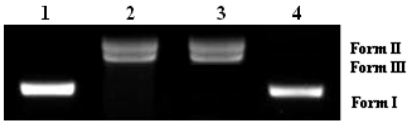

Fig. **11**. Lane 1, DNA control, Lane 2, DNA + Complex **1** (100 μM) in N_2 atmosphere, Lane 3, NC Form and linear form of DNA (obtained from DNA + **1**) as control without addition of T4 DNA ligase, Lane 4, conversion of NC and linear form (obtained from DNA + **1**) to SC form on treatment with 4 units of T4 ligase.

The cleavage reactions have been studied using different complex concentrations and incubation times. Fig. 12 shows the result of gel electrophoretic separations of plasmid pBR322 DNA induced by an increasing concentration of complex in the absence of external agents at pH = 7.2 (50 mM Tris-HCl buffer) and 37 ˚C for 3 h. With the increasing of the complex concentration, Form I plasmid DNA is gradually converted into Form II (lanes 2-4). When the concentration of complex **1** is added to 100 μM (lane 5), the Form I completely converted to Form II and Form III.

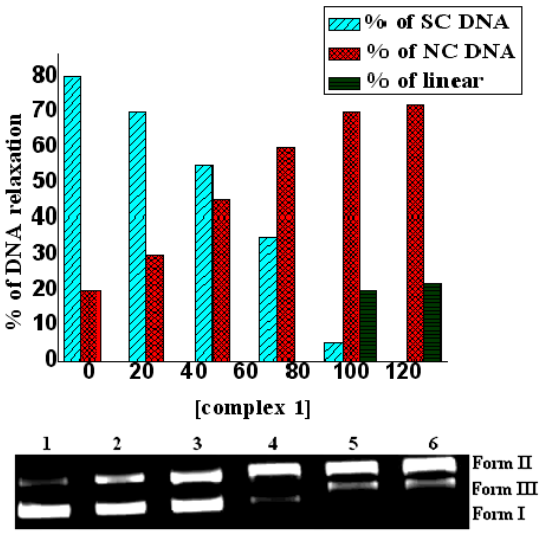

Fig. 12. Agarose gel showing cleavage of pBR 322 DNA incubated by complex **1** (various concentrations) in Tris–HCl buffer (pH = 7.2) at 37ºC for 3 h. Lane 1, DNA control, Lane 2, DNA + Complex **1** (25 μM), Lane 3, DNA + Complex **1** (50 μM), Lane 4, DNA + Complex **1** (75 μM), Lane 5, DNA + Complex **5** (100 μM), Lane 6, DNA + Complex **1** (125 μM).

The result indicates that the DNA cleavage activity of the complex is obviously complex concentration-dependent. In addition, a time course of a gel electrophoresis pattern of pBR322 DNA cleavage during a reaction in the presence of 100 μM complex at pH = 7.2 and 37˚C is shown in Fig. 13. With reaction time increase, the amount of Form II and Form III increased and Form I gradually disappeared. The result shows that the complex

5 can effectively cleave the pBR322 plasmid DNA in the absence of external agents, and the cleavage of DNA by the complex is dependent on the reaction time. From Fig. 14a, the disappearance of SC DNA and the formation of the NC DNA and linear with reaction time shown expected exponential nature of the curves. The plot of ln (% SC DNA) versus time (Fig. 14b) is linear, which indicates the process to be pseudo-first-order, this is consistent with the general model for enzyme catalyzed reactions.[28]

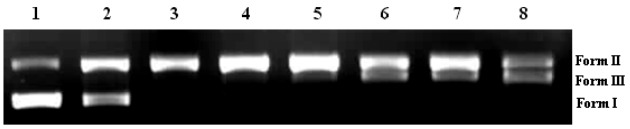

Fig. 13. Time-dependence of pBR322 DNA cleavage by 100 µM complex **5** in Tris-HCl/NaCl buffer (pH = 7.2) at 37 º C. Lane 1: DNA control (3 h), lane 2-8: DNA + **5** (0.25, 0.5, 1, 1.5, 2, 2.5, 3 h).

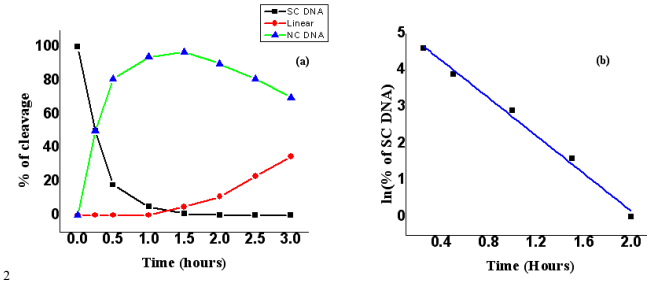

Fig. 14. (a) Disappearance of the super coiled form and formation of the nicked circular form of pBR322 DNA in the presence of the complex **5** (100 µM) with the incubation time (pH = 7.2, 37º C). (b) ln(% SC DNA) versus time for a complex **5** (100 µM).

Fitting the experimental data with first-order consecutive kinetic equations, the rate constant k_1 is obtained to be 6.9×10^{-4} s^{-1}, for the conversions of supercoiled to nicked and linear DNA. This cleavage rate value is two times higher than our early reported[12a] oxyimine based macrocyclic binuclear Ni(II) system, which showed 3.52×10^{-4} s^{-1}. By comparing the results of hydrolysis reactions catalysed by **5**, we can conclude that the macrocyclic ligand with the more aromatic moiety could play important roles in the DNA cleavage process.

3. Experimental

3.1 Materials and measurements

2,6-diformyl-4-methyl-phenol was prepared by following the literature method.[29] Tetra(*n*-butyl)ammonium perchlorate (TBAP) was purchased from Fluka and recrystallized from hot methanol. (**Caution:** TBAP is potentially explosive hence care should be taken in handling the compound). 2-aminobenzylamine was purchased from Aldrich. CT-DNA and pBR322DNA were purchased from Bangalore Genie (India). BSA (bovine serum albumin) was purchased from Sigma Company and was used without further purification and its molecular weight was assumed to be 68000. All BSA solutions were prepared in the Tris-HCl (pH=7.2) buffer and stocked at 4 °C. All other chemicals and solvents were of analytical grade and used as received. FTIR spectra were obtained on a Perkin Elmer FTIR spectrometer with samples prepared as KBr pellets. UV-Vis spectra were recorded using a Perkin Elmer Lambda 35 spectrophotometer operating in the range of 200-800 nm with quartz cells and ε are given in $M^{-1}cm^{-1}$. CH11008 Electrochemical analyzer using a three- electrode cell setup comprised of glassy carbon working, platinum wire auxiliary and saturated Ag/AgCl electrodes. The concentration of the complexes was 10^{-3} M and TBAP (10^{-1} M) was used as the supporting electrolyte. The emission spectra were recorded on Perkin Elmer LS-45 fluorescence spectrometer. Viscosity measurements were recorded using a Brookfield Programmable LV DVII+ viscometer. The electro spray mass spectra were recorded on a Q-TOF micro mass spectrometer.

3.2 Synthesis of mononuclear nickel(II) complex

3.2.1 Synthesis of mononuclear [NiL] complex.

To a solution of 2,6-diformyl-4-methyl-phenol (1.0 g, 6 mmol) in warm dimethyl formamide (10 ml), 2-aminobenzylamine (0.37 g, 3 mmol) in warm dimethyl formamide (10 ml) was added dropwise under constant stirring. To this solution $Ni(OAc)_2 \cdot 4H_2O$ (0.75 g; 3 mmol) was added and the nickel acetate dissolved immediately. The solution was stirred at 60 º C for 2 h. A brown colored mononuclear complex [NiL] precipitated. The solid was separated by filtration and washed with isopropyl alcohol and diethyl ether (0.6 g, 42%). Selected IR data (ν, cm^{-1}): 2915, 1668.37 and1619.

3.3 Synthesis of binuclear nickel(II) complexes

3.3.1 Synthesis of $[Ni_2L^1(H_2O)_2]2ClO_4$ (1)

The binuclear Ni(II) complex **1** was prepared from a vigorously stirred suspension of mononuclear complex NiL (0.5 g, 1 mmol) in methanol (25 ml), a methanolic solution of $Ni(ClO_4)_2 \cdot 6H_2O$ (0.39 g, 1 mmol) was added slowly and the mixture was stirred for 15 min to obtain a clear solution. Then the methanolic solution (5 ml) of 1,2-diaminoethane (0.06 g, 1 mmol) was added drop wise to the above solution and refluxed for 3 h. A resulting solid was separated on evaporating the solution up to 20 ml at room temperature. Reddish brown crystals suitable for X-ray analysis were obtained after several days by slow evaporation of acetonitrile solution (0.42 g 57 %). Anal. calcd (%) for $C_{27}H_{32}Cl_2N_4Ni_2O_{14}$: C 39.31, H 3.91, N 6.79. Found (%): C 39.48, H 3.98, N 6.88. ESI-MS in CH_3CN: *m/z*: 653 $[L^1 + 2Ni+ClO_4]^+$, 588 $[L^1 + 2Ni+2H_2O]^+$ and 277 $[L^1+2Ni]^{2+}$. Selected IR data (ν, cm^{-1}): 3336, 2927, 1627, 1116 and 630. UV-vis: λ_{max} (DMF)/ nm: 258 (90,000), 320 (35,000), 400 (23,000), 540 (75), 750 (40) and 920 (60).

3.3.2 Synthesis of $[Ni_2L^2(H_2O)_4].2ClO_4$ (2)

The complex **2** was synthesized by following the previously described procedure for complex **1**, using 1,3-diaminopropane instead of 1,2-diaminoethane. A red colour compound was obtained on evaporation of the solvent (0.4 g, 52 %). Anal. calcd (%) for $C_{28}H_{34}Cl_2N_4Ni_2O_{14}$: C 40.09, H 4.09, N 6.68. Found (%): C 40.17, H 4.15, N 6.73. ESI-MS in CH_3CN: *m/z*: 667 $[L^2 + 2Ni+ClO_4]^+$, 603 $[L^2 + 2Ni+2H_2O]^+$ and 284 $[L^2+2Ni]^{2+}$. Selected IR data (ν, cm^{-1}): 3348, 2920, 1636, 1080 and 629. UV-vis:

λ_{max}(DMF)/ nm: 228 (72,000), 258 (80,000), 382 (25,000), 566 (80), 777 (35) and 935 (55).

3.3.3 Synthesis of $[Ni_2L^3(H_2O)_4].2ClO_4$ (3)

The complex **3** was synthesized by following the previously described procedure for complex **1**, using 1,3-diaminobutane instead of 1,2-diaminoethane. An orange colour compound was obtained on evaporation of the solvent (0.37g, 47 %). Anal. calcd (%) for $C_{29}H_{36}Cl_2N_4Ni_2O_{14}$: C 40.84, H 4.25, N 6.57. Found (%): C 40.97, H 4.32, N 6.63. ESI-MS in CH_3CN: *m/z*: 681 $[L^3 + 2Ni+ClO_4]^+$, 617 $[L^3 + 2Ni+2H_2O]^+$ and 290 $[L^3+2Ni]^{2+}$. Selected IR data (ν, cm^{-1}): 3391, 2930, 1616, 1071 and 639. UV-vis: λ_{max}(DMF)/ nm: 260 (1,15,000), 308 (28,000), 366 (22,000), 575 (75), 780 (40) and 940 (60).

3.3.4 Synthesis of $[Ni_2L^4(H_2O)_4].2ClO_4$ (4)

The complex **4** was synthesized by following the previously described procedure for complex **1**, using 1,2-diaminobenzene instead of 1,2-diaminoethane. A reddish brown colour compound was obtained on evaporation of the solvent (0.45 g, 56 %). Anal. calcd (%) for $C_{31}H_{32}Cl_2N_4Ni_2O_{14}$: C 42.65, H 3.70, N 6.42. Found (%): C 42.72, H 3.75, N 6.47. ESI-MS in CH_3CN: *m/z*: 701 $[L^4 + 2Ni+ClO_4]^+$, 636 $[L^4 + 2Ni+2H_2O]^+$ and 300 $[L^4+2Ni]^{2+}$. Selected IR data (ν, cm^{-1}): 3350, 2928, 1640, 1080 and 626. UV-vis: λ_{max} (DMF)/ nm: 240 (28,000), 310 (32,000), 380 (22,000), 460 (14,000), 545 (78), 752 (25) and 920 (60).

3.3.5 Synthesis of $[Ni_2L^5(H_2O)_4].2ClO_4$ (5)

The complex **5** was synthesized by following the previously described procedure for complex **1**, using 1,8-diaminonahthalene instead of 1,2-diaminoethane. A brown colour compound was obtained on evaporation of the solvent (0.4 g, 47 %). Anal. calcd (%) for $C_{35}H_{34}Cl_2N_4Ni_2O_{14}$: C 45.55, H 3.71, N 6.07. Found (%): C 45.62, H 3.76, N 6.15. ESI-MS in CH_3CN: *m/z*: 751 $[L^5 + 2Ni+ClO_4]^+$, 687 $[L^5 + 2Ni+2H_2O]^+$ and 326 $[L^5+2Ni]^{2+}$. Selected IR data (ν, cm^{-1}): 3381, 2925, 1638, 1086 and 627. UV-vis: λ_{max} (DMF)/ nm: 225 (1,20,000), 430 (50,000), 550 (70), 780 (30) and 940 (55).

3.4 X-Ray diffraction

Single crystal with appropriate unit cell dimensions was used for Crystallographic structure analysis. The X-ray intensity were collected at 293 K with a Bruker SMART APEX II area detector diffractometer using Mo-Kα radiation (λ = 0.71073 Å) with the ω and ϕ scan technique. The structure was solved by direct methods (SHELXS 97) [30] and refined using SHELXL 97 by least square technique on F^2. The hydrogen atoms were positioned geometrically and refined with fixed thermal displacement parameters.

3.5 DNA binding experiments

Absorption spectral titrations were carried out in (50 mM Tris-HCl buffer, pH 7.2) buffer at room temperature to investigate the binding affinity between CT-DNA and complex. The concentration of CT-DNA was determined from the absorption intensity at 260 nm with a ε value[31] of 6600 $M^{-1}cm^{-1}$. Absorption titration experiments were performed by varying the concentration of the CT-DNA (0-200 μM) keeping the complex concentration (10 μM) as constant. The absorbance (A) was recorded after each addition of CT-DNA. In order to eliminate the absorbance of the CT-DNA an equal amount of the same was added to both the compound solution and the reference solution. The intrinsic binding constant, K_b for the complexes **1-5** was determined from the spectral titration data using the following equation.[32]

$$[DNA]/(\varepsilon_a - \varepsilon_f) = [DNA]/(\varepsilon_b - \varepsilon_f) + 1/K_b(\varepsilon_b - \varepsilon_f) \quad (1)$$

Here, ε_a, ε_f, and ε_b, corresponds to A_{obsd} / [Ni(II) complex], extinction coefficient for the free complex, and extinction coefficient for the complex in the fully bound form, respectively.

The relative binding of complexes **1-5** to CT-DNA was studied with an EB-DNA solution in Tris-HCl buffer (pH 7.2). Fluorescence intensities at 610 nm (exited at 510 nm) were measured at different complex concentrations. The reduction of emission intensity gives a measure binding propensity of complex to CT-DNA. Stern-Volmer quenching constant K_{sv} of the complexes **1-5** to CT-DNA were determined from the equation $I_o/I=1 + K_{sv}r$ where I_o and I are fluorescence intensities of EB-DNA in absence and presence complex, respectively. K_{sv} is a linear Stern- Volmer quenching constant. r is the ratio of the total concentration of complex to that of DNA, [M]/[DNA]. In the linear fit plot of I_0/I *vs.* [complex]/[DNA], K_{sv} is given by the ratio of the slope to intercept. The apparent binding constant (K_{app}) was calculated using the equation $K_{EB}[EB]/K_{app}[complex]$ where K_{EB} = 1 x 10^7, [EB] = 4 μM, and [complex] is the concentrations of the complex at 50% reduction of the emission intensity of EB.[33] To further clarify the binding mode of the present nickel complexes to CT-DNA, viscosity measurements were carried out on CT-DNA (0.5 mM) by varying the concentration of the added complexes (0.01 mM, 0.02 mM, 0.03 mM, 0.04 mM, 0.05 mM). Data were presented as (η/η_o) versus binding ratio of concentration of complex to that of concentration of CT-DNA , where η is the viscosity of DNA in the presence of complex and η_o is the viscosity of DNA alone.

3.6 Protein binding studies

Fluorescence spectra were recorded from 300 to 500 nm with the excitation wavelength at 280 nm. First 3 ml of solution containing an appropriate concentration (~1 μmol/L) of BSA was titrated by the successive addition of binuclear nickel (II) complex solution. Titrations were done manually via a micro syringe and the fluorescence intensity of BSA in the absence and the presence of the complex was measured after incubation for 5 min. All experiments were measured at room temperature. Under strictly controlled temperature and pH value, the cause of fluorescence quenching mode is, as below, dynamic or static quenching. In order to determine the quenching property, the fluorescence decay data were analyzed via the Stern-Volmer equation.[34]

$$F_0/F=1+ K_{sv}[Q] \quad (2)$$

Where F_0 and F are steady-state fluorescence intensities in the absence and the presence of quencher, respectively. K_{sv} is the Stern-Volmer quenching constant and [Q] is the concentration of

quencher. The plot of F_0 /F vs [Q] shows the value of K_{SV}. According to the equation:

$$K_{SV} = K_q\tau_0 \quad (3)$$

where K_q is the quenching rate constant and τ_0 is the fluorescence life time of protein in the absence of quencher, the value of τ_0 is considered to be 10^{-8} s.

When small molecules bind independently to a set of equivalent sites on a macromolecule, the equilibrium between free and bound molecules is given by the equation.[35]

$$\log (F_0 - F)/F = \log K + n \log [Q] \quad (4)$$

Where K is the binding constant to a site and n is the number of binding sites per BSA. The binding constant K and the number of binding sites n can be obtained by using Eq. (4). The UV measurements of BSA in the presence and the absence of binuclear Ni(II) complex were made in a range of 200 - 500 nm. BSA concentrations were fixed at 10 µmol/L. The influences of the absorbance of binuclear Ni(II) complexes were eliminated by adding in the reference cells the solutions of binuclear Ni(II) complexes of the same concentrations as in the sample solution.

3.7 DNA cleavage experiments

The DNA cleavage experiments were done by agarose gel electrophoresis. pBR 322 DNA (0.1µg/µl) in Tris-buffer (pH 7.2) was treated with complexes. The sample was incubated for a 3 h at 37 ºC and the reaction quenched by 1 µl of loading buffer. pBR 322 DNA bands were stained by EB, visualized under UV light and photographed. The extent of cleavage of SC DNA was determined by measuring the intensities of the bands using a UVITECH Gel Documentation System. To investigate the mechanism of DNA cleavage in the presence of hydroxyl radical scavengers (DMSO, KI), singlet oxygen quenchers (L-histidine, NaN_3), superoxide scavenger (superoxide dismutase enzyme SOD) and chelating agent (EDTA) under our experimental conditions. Kinetics Analysis were carried out at fixed concentrations of DNA and complex **1** (100 µM) with different incubation times under identical experimental conditions.

4. Conclusions

A series of macrocyclic binuclear nickel(II) complexes have been synthesized and their electrochemical, DNA, BSA binding and DNA hydrolysis were also evaluated. Introducing and extending the aromatic moiety in the macrocyclic ring led to considerable changes in DNA binding mode and hydrolysis rate under physiological conditions. The complex **5** displayed higher DNA binding propensity (intercalative mode) and cleavage activity than the other binuclear nickel(II) analogues. Thus, the stacking interaction exhibited by the naphthalene diimine containing macrocyclic ligand L^5, which is responsible for the stronger DNA intercalative binding, more effective DNA cleavage of the complex in the absence of any additives. All the complexes can cleave the DNA through hydrolytically, because a hydroxyl radical scavengers (DMSO, KI), singlet oxygen quenchers (L-histidine, NaN_3) and superoxide scavenger (SOD) was completely ineffective in the cleavage activity. The rate constant k_1 is obtained to be 6.9×10^{-4} s^{-1} for the conversions of supercoiled to nicked and linear DNA by napthalenediimine containing macrocyclic Ni(II) complex **5**. BSA binding experimental results suggested that these Ni(II) complexes could bind to the serum albumins by high affinity and quench the fluorescence of serum albumins through a static quenching mechanism. This reveals that a synergic combination of the ligand and metal ion is important in the design of a potential DNA and BSA interacting agent.

References

1 J. Qing, H. Daghriri and P. Beale, *J. Inorg. Biochem.,* 2004, **98**, 1261.

2 A. Nori and J. Kopecek, *Adv. Drug Deliv. Rev.,* 2005, **57**, 609.

3 Y. Xie, G. G. Miller, S. A. Cubitt, K. J. Soderlind, M. J Allalunis-Turner and J. W. Lown, *Anticancer Drug Des.,* 1997, **12**, 169.

4 M. Shi, K. Ho, A. Keating and M. S. Shoichet, *Adv. Funct. Mater*., 2009, **19**, 1689.

5 D. D. Van Ho, R. Schilsky and C. M. Reichert, *Cancer Treat. Rep.,* 1979, **63,** 1527.

6 E. R. Jamieson and S. J. Lippard, *Chem. Rev.,* 1999, **99**, 2467.

7 S. Komeda, M. Lutz, A. L. Spek, M. Chikuma and J. Reedijk, *Inorg. Chem*., 2000, **39**, 4230.

8 O. Novakova, J. Kasparkova, O. Vrana, P. M. Van Vliet, J. Reedijk and V. Brabec, *Biochemistry,* 1995, **34**, 12369.

9 E. L. Hegg and J. N. Burstyn, *Coord. Chem. Rev.,* 1998, **173**, 133.

10 (a) Q. X. Yang, L. Z. Gang, L. W. Sheng and Z. H. Liang, *Chinese J. Struct. Chem.*, 2008, **27**, 707. (b) C. S. Liu, H. Zhang, R. Chen, X. S. Shi, X. H. Bu and M. Yang, *Chem. Pharm. Bull.*, 2007, **55**, 996. (c) P. Krishnamoorthy, P. Sathyadevi, R. R. Butorac, A. H. Cowley, N. S. P. Bhuvanesh and N. Dharmaraj, Dalton Trans., 2012, **41**, 4423.

11 (a) O. A. EI Gammal, G. M. Abu El Reash and M. M. El Gamil, *Spectrochim. Acta A*, 2012, 96C, 444. (b) R. Prabhakaran , P. Kalaivani , P. Poornima , F. Dallemer , G. Paramaguru , V. Vijaya Padma , R. Renganathan , R. Huang and K. Natarajan, *Dalton Trans.*, 2012, **41**, 9323.

12 (a) S. Anbu, M. Kandaswamy and B. Varghese, *Dalton Trans.*, 2010, **39**, 3823. (b) S.Anbu, S. Shanmugaraju and M. Kandaswamy, *RSC Advances*, 2012, **2**, 5349.(c) S. Anbu, M. Kandaswamy, P. Suthakaran, V. Murugan and B. Varghese, *J. Inorg. Biochem.*, 2009, **103**, 401. (d) L. Leelavathy, S. Anbu, M. Kandaswamy, N. Karthikeyan and N. Mohan, *Polyhedron*, 2009, **28**, 903. (e) S. Anbu, M. Kandaswamy, P. S. Moorthy, M. Balasubramanian and M. N. Ponnuswamy, *Polyhedron*, 2009, **28**, 49. (f) S. Anbu and M. Kandaswamy, *Polyhedron*, 2011, **30**, 123. (g) S. Anbu, M. Kandaswamy and M. Selvaraj, *Polyhedron*, 2012, **33**, 1. (h) S. Anbu and M. Kandaswamy, *Inorg. Chim. Acta*, 2012, **385**, 45.

13 (a) S. Anbu, S. Kamalraj, B.Varghese, J. Muthumary and M. Kandaswamy, *Inorg. Chem.*, 2012, **51**, 5580. (b) S. Anbu, R. Ravishankaran, A. A. Karande and M. Kandaswamy, Dalton Trans., 2012, **41**, 12970.

14 (a) D.C. Carter and J. X. Ho, *Adv. Protein Chem.,* 1994, **45,** 153. (b) Y. Z. Zhang, J. Dai, X. Xiang, W. W. Li and Y. Liu, *Mol. Biol. Rep.,* 2010, **37**, 1541.
15 A. Sulkowska, *J. Mol. Struct.,* 2002, **614**, 227.
16 Y. Z. Zhang, B. Zhou, Y. X. Liu, C. X. Zhou, X. L. Ding and Y. J. Liu, *Fluoresc.,* 2008, **18**, 109.
17 (a) D. Volkmer, B. Hommerich, K. Griesar, W. Haase and B. Krebs, *Inorg.Chem.,* 1996, **35**, 3792. (b) M. Ciampolini, *Inorg. Chem.,* 1966, **5**, 35.
18 L. Sacconi, M. Ciampolini and G. P. Speroni, *J. Am. Chem. Soc.,* 1965, **87**, 3102.
19 (a) S. Akine, T. Taniguch and T. Nabeshima, *Chem. Lett.,* 2001, 682. (b) R. Das and K. Nag, *Inorg. Chem.,* 1991, **30**, 2831.
20 (a) M. M. Bhadbhade and D. Srinivas, *Inorg. Chem*., 1993, **32** 6122.(b) S. K. Mandal and K. Nag, *J. Chem. Soc.*, *Dalton Trans.*, 1983, 2429. (c) W. E. Gao, G. Bu, D. Yang, Z. Liao, S. Jiang, G. Yan and J. Way, *J. Chem. Soc., Dalton Trans.*, 2000, 1431. (d) J. Manonmani, R. Thirumurugan, M. Kandaswamy, V. Narayanan, V. Shanmugasundara Raj, M. N. Ponnuswamy, G. Shanmugam and H. K. Fun, *Polyhedron,* 2001, **20**, 3039.
21 M. Thirumavalavan, P. Akilan and M. Kandaswamy, *Supramol. Chem.*, 2004, **16(7)**, 495.
22 F. J. Megar Almes and D. Porschke, *Biochemistry,* 1993, **32**, 4246.
23 R. F. Pasternack, M. Cacca, B. Keogh, T. A. Stephenson, A. P. Williams and F. J. Gibbs, *J. Am. Chem. Soc*., 1991, **113,** 6835.
24 M. R. Eftink and C. A. Ghiron, *Anal. Biochem.*, 1981, **114**, 199.
25 M. R Eftink and C. A. Ghiron, *J. Phys. Chem*., 1976, **80**, 486.
26 L. A. Basile and J. K. Barton, J. Am. Chem. Soc., 1987, **109**, 7548.
27 (a) A. Sreedhara and J. D. Cowan, *Chem. Commun.*, 1998, 1737, (b) S. Dhar, P. A. N. Reddy and A. R. Chakravarty, *Dalton Trans.*, 2004, 697.
28 (a) D. M. Kong, J. Wang, L. N. Zhu, Y. W. Jin, X .Z. Li and H. X. Shen, *J. Inorg. Biochem*., 2008, **102**, 824. (b) J. J. Li, R. Geyer and W. Tan*, Nucleic Acids Res*., 2000,**28**, e52.
29 N. V. Verani, E. Rentschler, T. Weyhermuller, E. Bill and P. Chaudhuri, *J. Chem. Soc*., *Dalton Trans.*, 2000, 251.
30 G. M. Sheldrick, *Acta Cryst*., **2008**, A64, 112.
31 M. E. Reichmann, S. A. Rice, C. A. Thomas and P. Doty, *J. Am. Chem. Soc.*, **1954**, 76, 3047.
32 A. Wolfe, G. H. Shimer and T. Mechan, *Biochemistry*, **1987**, 26, 6392.
33 Y. Zhao, J. Zhu, W. He, Z. Yang, Y. Zhu, Y. Li, J. Zhang and Z. Guo, *Chem. Eur. J.*, 2006, **12**, 6621.
34 M. R. Eftink and C. A. Ghiron, *Anal. Biochem.*, 1981, **114**, 199.
35 H. Gao, L. Lei, J. Liu, K. Qin, X. Chen and Z. Hu, *J Photochem. Photobiol., Part A*, 2004, **167**, 213.